RESEARCH ARTICLE OPEN ACCESS

Temperature-Resolved Fluorescence Quenching on Ultrasmall Gold Nanoparticles Conjugated with Dye-Labeled Peptides

Lisa-Sofie Wagner[1] | Alexander Huber[2] | Kateryna Loza[1] | Christine Beuck[3] | Marc Heggen[4] | Peter Bayer[3] | Jens Voskuhl[2] | Matthias Epple[1]

[1]Inorganic Chemistry and Center for Nanointegration Duisburg-Essen (CENIDE), University of Duisburg-Essen, Essen, Germany | [2]Organic Chemistry, Center for Medical Biotechnology (ZMB) and Center for Nanointegration Duisburg-Essen (CENIDE), University of Duisburg-Essen, Essen, Germany | [3]Institute of Biology and Center for Medical Biotechnology (ZMB), University of Duisburg-Essen, Essen, Germany | [4]Ernst Ruska Centre for Microscopy and Spectroscopy with Electrons, Jülich, Germany

Correspondence: Matthias Epple (matthias.epple@uni-due.de)

Received: 31 March 2025 | **Revised:** 24 June 2025 | **Accepted:** 25 June 2025

Funding: The authors received no specific funding for this work.

Keywords: nanoparticles | fluorescence | gold | quantum yield | quenching | ultrasmall

ABSTRACT

Fluorescent peptides were covalently attached to the surface of ultrasmall gold nanoparticles (2 nm), that is, FITC-AlaCys, FITC-Ala-Ala-Ala-Cys, and Trp-Ala-Cys (WAC). For comparison, the fluorescent dye AlexaFluor-647 was attached to glutathione-coated gold nanoparticles via click chemistry. Each particle carried between 10 and 20 fluorescent ligands, except for WAC where about 60 peptides were attached to each nanoparticle. The photophysical properties of dissolved and nanoparticle-conjugated dyes were assessed by UV-Vis and fluorescence spectroscopy, including measurements of the absolute photoluminescence quantum yields at the same dye concentration. After conjugation to the nanoparticles, the quantum yield decreased by a factor of 10 to 20 in the FITC systems but only by a factor of 1.5 in the AlexaFluor-647 system. The intrinsic fluorescence was almost completely lost for WAC after conjugation to the nanoparticles. The fluorescence intensity at temperatures up to 85°C showed a decrease with temperature in all cases which was stronger for dissolved dyes than for nanoparticle-conjugated dyes. The fluorescence was fully recovered after cooling back to ambient temperature, that is, there was no permanent change of the particles caused by heating.

1 | Introduction

Metallic nanoparticles are of considerable importance in various scientific areas, for example, in heterogeneous catalysis or biomedicine [1–5]. Their synthesis is now very advanced, with many (usually noble) metals and their alloys available as core material. Nanoparticles with a diameter of 10–15 nm show a typical surface plasmon resonance that gives gold colloids their classical red color [6]. The absorption and emission near the optical range can also be used to prepare metal nanoparticles for the absorption of NIR radiation, for example, for local tumor thermotherapy [7–10]. Ultrasmall metal nanoparticles with a diameter of 1–3 nm are much smaller and do not show a plasmon resonance [1, 11–16]. On the other hand, they do not quench the fluorescence of attached ligands, unlike plasmonic metal nanoparticles that cannot be fluorescently labeled due to strong quenching [6]. Thus, they can be used as fluorescent probes, for example, in cell culture or in tissues [17–20]. Along the same line, ultrasmall nanoparticles can be analyzed by NMR spectroscopy in dispersion, which is impossible for plasmonic

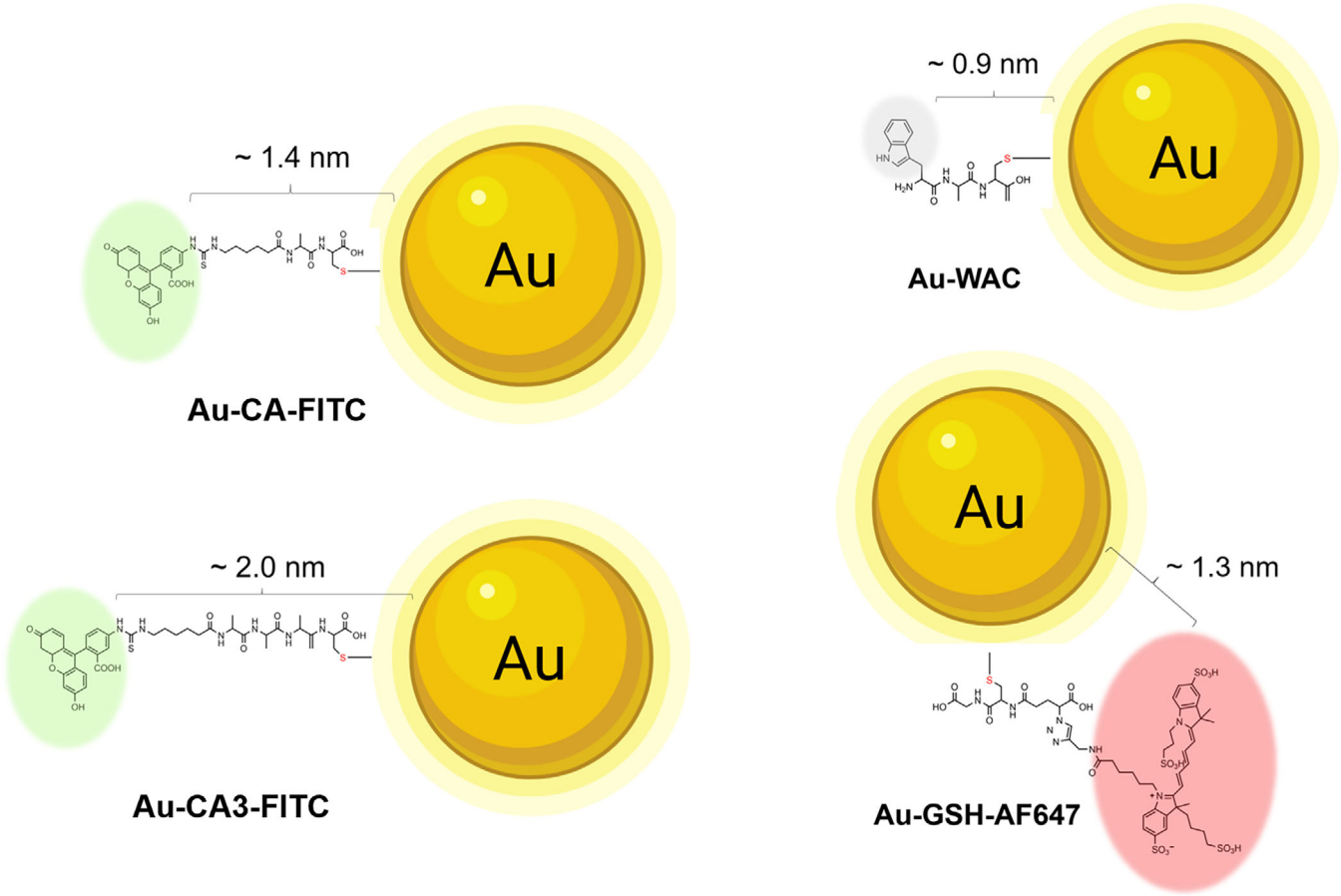

FIGURE 1 | Schematic picture of ligand-conjugated ultrasmall gold nanoparticles, drawn to scale. The estimated distance between the gold surface and the fluorophore is indicated, assuming an expanded conformation of the connecting ligand.

nanoparticles [21–23]. This opens a convenient way to analyze the ligand shell around the metal core and to quantify the number of attached ligands [24]. If the ligands are UV-Vis absorbing, they can also be quantified by UV-Vis spectroscopy by application of Lambert-Beer's law [25].

Considerable efforts have been devoted to understanding the optical behavior of gold nanoparticles with attached dyes [10, 26–30]. It was demonstrated for large gold nanoparticles (5 to 10 nm) that plasmonic interactions lead to strong quenching of an attached fluorophore, with the nanoparticles absorbing the excitation energy of the dye and converting it into heat [31, 32]. This was observed for molecules that are close to the metal core [30, 32, 33]. In that case, fluorescence quenching occurs mainly by non-radiative deactivation pathways. However, it was also shown that the emission can be increased by the presence of a metal nanoparticle core. In particular, larger nanoparticles (>20 nm) with attached fluorophores showed a significant emission enhancement. Plasmonic gold nanoparticles (>3 nm) can enhance the local electromagnetic field. This amplification can intensify the absorption and emission of the fluorophore, increasing the fluorescence signals. The ideal distance between fluorophore and nanoparticle surface for this amplification is about 5–10 nm [33, 34]. Chhabra et al. studied the dependence of the fluorescence intensity on the distance to the metal core on gold nanoparticles of 5 or 10 nm diameter by adjusting the distance between the nanoparticle and fluorophore with rigid DNA oligonucleotides. Notably, a strong quenching was observed below a distance of 5 nm [32]. It was demonstrated that the quenching decreases with about d^{-4} with d the distance between the metal surface and the fluorophore [26, 32, 35].

Fluorescently labeled peptides [36, 37], nucleic acids [38], nanobodies [39], and precision polymers [40] have all been covalently attached to the surface of ultrasmall gold nanoparticles. Fluorescent dyes have been conjugated to the surface of ultrasmall gold, platinum, and silver-platinum nanoparticles via click chemistry, for example, to follow the nanoparticle pathway inside cells [41]. However, the photochemistry of fluorescently labeled molecules that are attached to ultrasmall nanoparticles has not yet been studied in detail. A practically important aspect is the degree of quenching by the metal core, as this determines the efficiency of fluorescent labeling, a decisive factor if such nanoparticles are prepared as theranostic probes. Clearly, the distance between the metal surface and the fluorophore is important.

Here, we report on a quantitative spectroscopic study where fluorescently labeled peptides were covalently attached to the surface of ultrasmall gold nanoparticles via a terminal cysteine. In addition, a tripeptide containing the fluorescent amino acid tryptophan or the classical dye AlexaFluor-647 was attached to

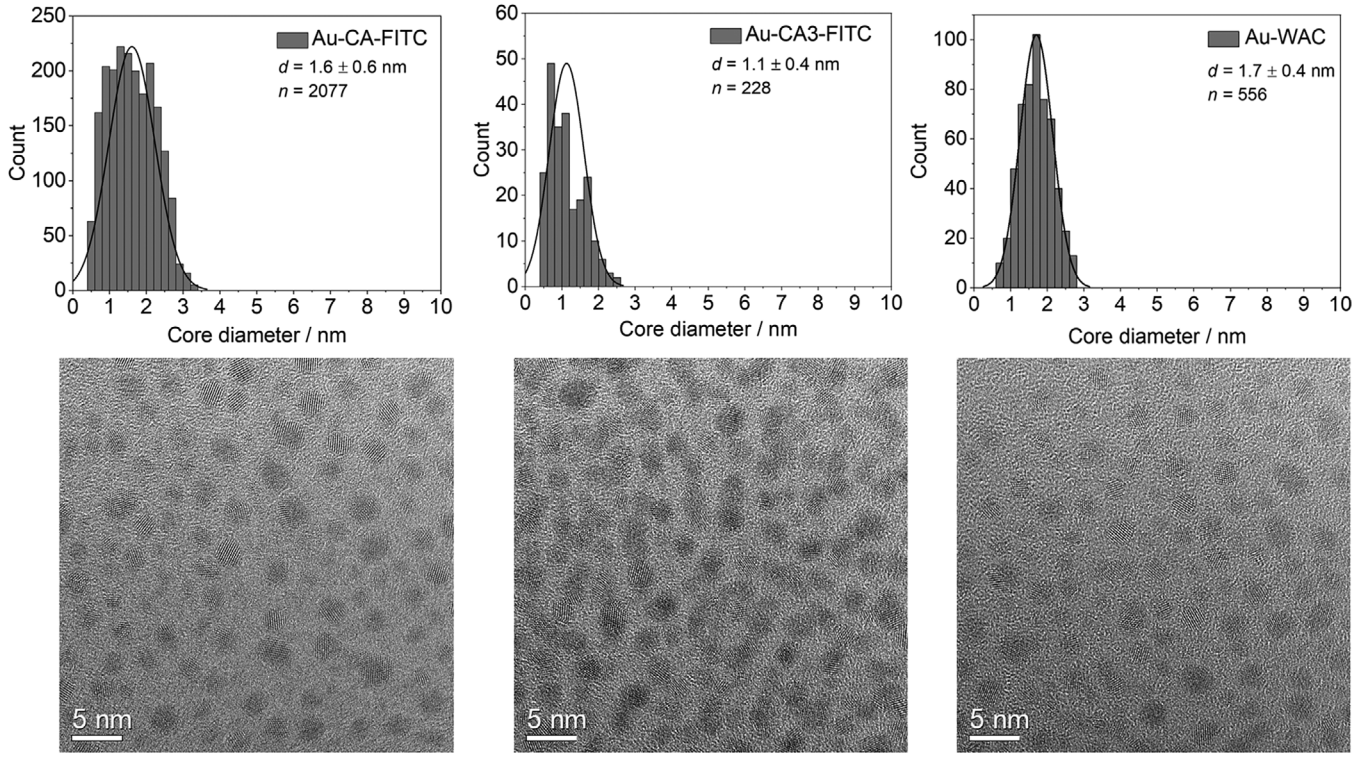

FIGURE 2 | HRTEM images of peptide-conjugated ultrasmall gold nanoparticles with corresponding particle size distribution (Au-CA-FITC, Au-CA3-FITC, and Au-WAC), determined by a machine learning approach [43]. The Au-GSH-AF647 nanoparticles had an average diameter of 2.5 ± 1.1 nm, as reported earlier (see Ref. [24] for the corresponding HRTEM image).

gold nanoparticles. Fluorescence intensities were measured, also as a function of temperature, and related to the nature of the dye. Absolute photoluminescence quantum yields gave a quantitative view. All particles were characterized in-depth, including the number of fluorescent molecules on each nanoparticle. This is imperative to obtain quantitative photophysical data at the same dye concentrations.

2 | Materials and Methods

2.1 | Reagents

Tetrachloroauric acid was prepared by the dissolution of elemental gold in *aqua regia*. Hydrochloric acid (HCl, 37%) and nitric acid (HNO_3, 67%) were obtained from Bernd Kraft (Duisburg, Germany). The peptides FITC-alanine-cysteine (denoted as CA-FITC in the following), FITC-alanine-alanine-alanine-cysteine (denoted as CA3-FITC in the following), and tryptophan-alanine-cysteine (denoted as WAC in the following) were obtained from Caslo (Kongens Lyngby, Denmark). The sequences are given from N- to C-terminus, but the short abbreviations used in this manuscript start with the cysteine to indicate the binding sequence from the gold surface. Sodium borohydride ($NaBH_4$, >96%) and 3 kDa spin filters were obtained from Merck (Darmstadt, Germany). Deuterium oxide (D_2O, 99.9%) was obtained from Deutero GmbH (Kastellaun, Germany). Ultrapure water (Purelab Flex 2 Ultra, 18.2 MΩ, ELGA) was used for all syntheses and characterizations.

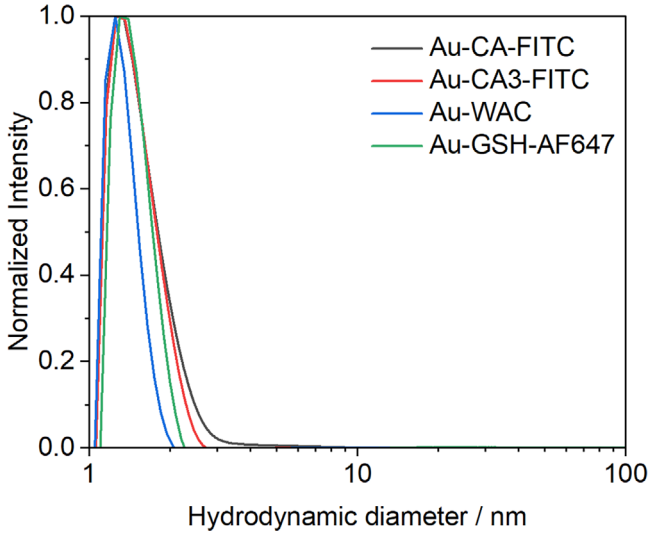

FIGURE 3 | Differential centrifugal sedimentation (DCS) of peptide-conjugated ultrasmall gold nanoparticles. Neither aggregates nor larger aggregates were present.

2.2 | Methods and Instruments for Characterization

Differential centrifugal sedimentation (DCS) was performed on a CPS Instruments DC disc centrifuge (24 000 rpm). Dodecane (0.5 mL) was used to prevent evaporation, and polyvinyl chloride particles with a defined size of 483 nm provided by CPS were

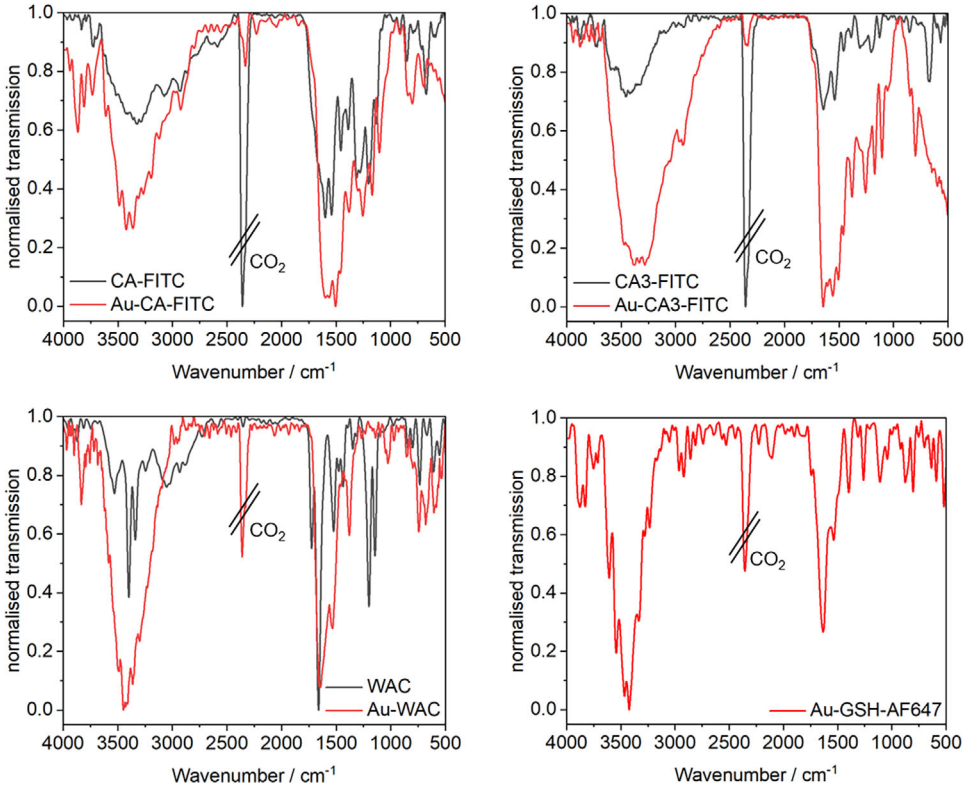

FIGURE 4 | Infrared spectra of ligands (black) and dried nanoparticles (red), showing the presence of the conjugated peptides.

used as calibration standard. HRTEM was performed with an aberration-corrected FEI Titan transmission electron microscope equipped with a Cs-probe corrector (CEOS Company) at a voltage of 300 kV [42]. The program ANTEMA was used to determine the particle size distribution [43]. Infrared spectroscopy was performed on dried nanoparticles in KBR pellets with a Vertex 70 spectrometer (Bruker). UV-Vis measurements were performed with a Genesis 50 instrument (Thermo Scientific) from 200 to 800 nm in a 600 µL quartz cuvette. A Cary Eclipse spectrometer (Agilent Technologies, Santa Clara, CA, USA) was used for fluorescence spectroscopy in quartz glass cuvettes (600 µL sample volume). Absolute photoluminescence quantum yields were determined in quartz glass cuvettes (600 µL sample volume) with an RF-6000 spectrofluorometer (Shimadzu Corporation, Japan) equipped with an ISR-6000 integrating sphere. The excitation wavelengths were as follows: CA-FITC and CA3-FITC: 491 nm; AF647: 645 nm; WAC: 280 nm.

Atomic absorption spectroscopy (AAS) was performed with a Thermo Electron M-Series spectrometer (graphite tube furnace; operated according to DIN EN ISO/IEC 17025:2005) to determine gold concentrations. For this, 10 µL of a nanoparticle dispersion was dissolved in 990 µL *aqua regia* and diluted with 4 mL water.

For NMR spectroscopy, the particles were dispersed in 540 µL H_2O/60 µL D_2O. All measurements were performed with a Bruker Avance Neo 400 MHz spectrometer with water suppression. DOSY measurements were carried out on a Bruker Avance III 700 MHz spectrometer equipped with a cryo-probe [36].

2.3 | Synthesis of Gold Nanoparticles

All particles were synthesized according to a modified Brust-Schiffrin synthesis [44]. Briefly, tetrachloroauric acid (20 µmol, 3.94 mg Au) was added to 50 mL degassed water. The corresponding peptide (60 µmol) was dissolved in 1 mL water and then quickly added to the reaction mixture. A decolorization of the reaction solution occurred. After 10 min stirring, 6.06 mg of sodium borohydride (160 µmol) dissolved in 800 µL ice-cold water was quickly added, resulting in a brown color of the dispersion. The particles were isolated by spin filtration in 3 kDa Amicon spin filters at 4000 rpm (2500 *g*) for 40 min and then washed seven times with water. Although no systematic study on the ratio of peptide to gold was performed here, the high stoichiometric excess of peptide to gold (about 3:1 = *n*:*n*) probably leads to the maximum surface coverage of peptides on the particle surface. The dye AlexaFluor-647 (AF647) was attached to the surface of glutathione-functionalized gold nanoparticles via copper-catalyzed azide-alkyne cycloaddition (CuAAC; click chemistry), as reported earlier [24, 38, 41].

3 | Results and Discussion

Two labeled peptides were selected, and the distance between the fluorophore and the metal core was adjusted by the length of the peptide chain. The ligands were FITC-Ala-Cys (CA-FITC) and FITC-Ala-Ala-Ala-Cys (CA3-FITC). In addition, the fluorescent peptide Trp-Ala-Cys (WAC) and the fluorescing dye AlexaFluor647 were attached to the nanoparticles, the latter via

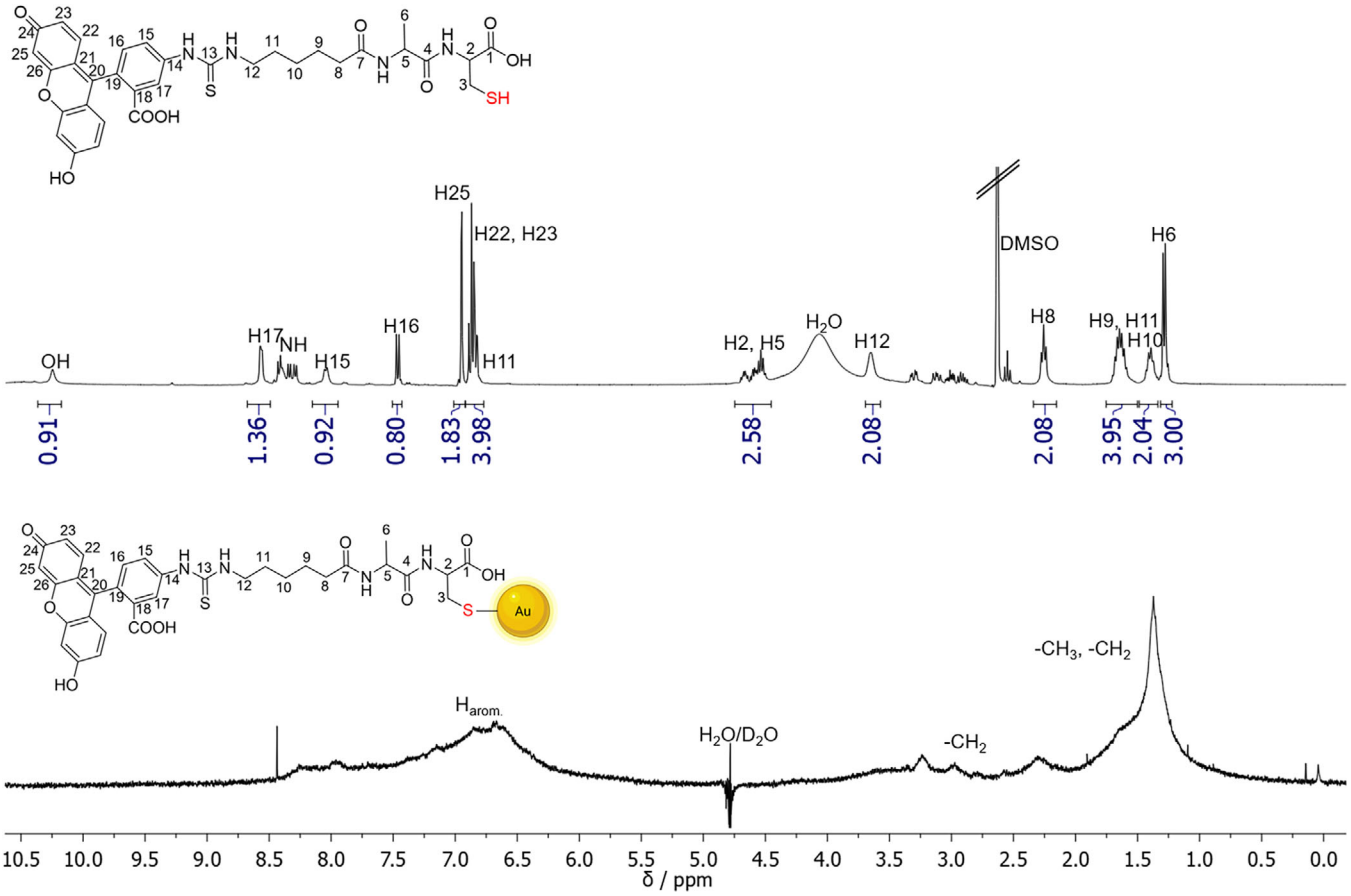

FIGURE 5 | ^{1}H NMR spectra of the ligand CA-FITC dissolved in DMSO-d_6 (top) and of Au-CA-FITC nanoparticles dispersed in 10% D_2O/90% H_2O (bottom). The spectra were measured at ambient temperature at 400 MHz.

click chemistry on glutathione (GSH)-terminated nanoparticles. Thus, our investigation comprised two peptides with FITC, one with the autofluorescent tripeptide WAC, one with AF647, and all corresponding nanoparticles. WAC was chosen for comparison because the amino acid tryptophan is intrinsically fluorescent. All gold nanoparticles investigated here are shown schematically in Figure 1. The nominal distance of the fluorophore to the surface of the gold nanoparticle varied between 0.9 and 2 nm, not considering a possible backfolding of the ligands towards the nanoparticle surface. However, as the surface is densely coated with ligands, we can tentatively assume that the dye is approximately in the distance from the surface, as depicted in Figure 1. Of course, this is only a rough assumption; in reality, there is probably a mixture of molecules in various configurations on each nanoparticle so that the average distance between the metal surface and the fluorophore is smaller than estimated in Figure 1.

The particles were analyzed with respect to their size and functionalization by high-resolution transmission electron microscopy (HRTEM), DCS, UV-Vis spectroscopy (UV-Vis), and ^{1}H NMR spectroscopy in dispersion, including diffusion-ordered NMR spectroscopy (DOSY). Furthermore, the temperature-dependent fluorescence and the absolute photoluminescence quantum yield were determined.

HRTEM was used to determine the metal core diameters of the particles (Figure 2). The particle size distribution was analyzed using the program ANTEMA [43]. All particles showed a monomodal size distribution with spherical particles. The average particle diameters were all below 2 nm, that is, all particles were ultrasmall. Similar results were reported earlier for ultrasmall gold nanoparticles functionalized with the unlabeled peptides CA and CA3. Here, the core diameters were 2.07 nm (Au-CA) and 2.15 nm (Au-CA3) [45].

The hydrodynamic diameter was determined by DCS. Monomodal particle size distributions with average hydrodynamic diameters of 1.2 to 1.3 nm were found (Figure 3). The hydrodynamic diameters of 1.5 nm for Au-CA-FITC and 1.3 nm for Au-CA3-FITC nanoparticles agree well with earlier results on gold nanoparticles carrying the unlabeled peptides CA and CA3 [45]. Very similar results were found for Au-WAC nanoparticles. The Au-GSH-AF647 nanoparticles had an average diameter of 1.4 ± 0.3 nm, in agreement with earlier results of (1.4 ± 0.2 nm) [24]. However, it is important to note that the diameter of ultrasmall particles is systematically underestimated by DCS as the method assumes the density of the metal core and not the actual density of the hydrated particles including the ligand shell, therefore resulting in an overestimation of the density and consequently an underestimation of particle

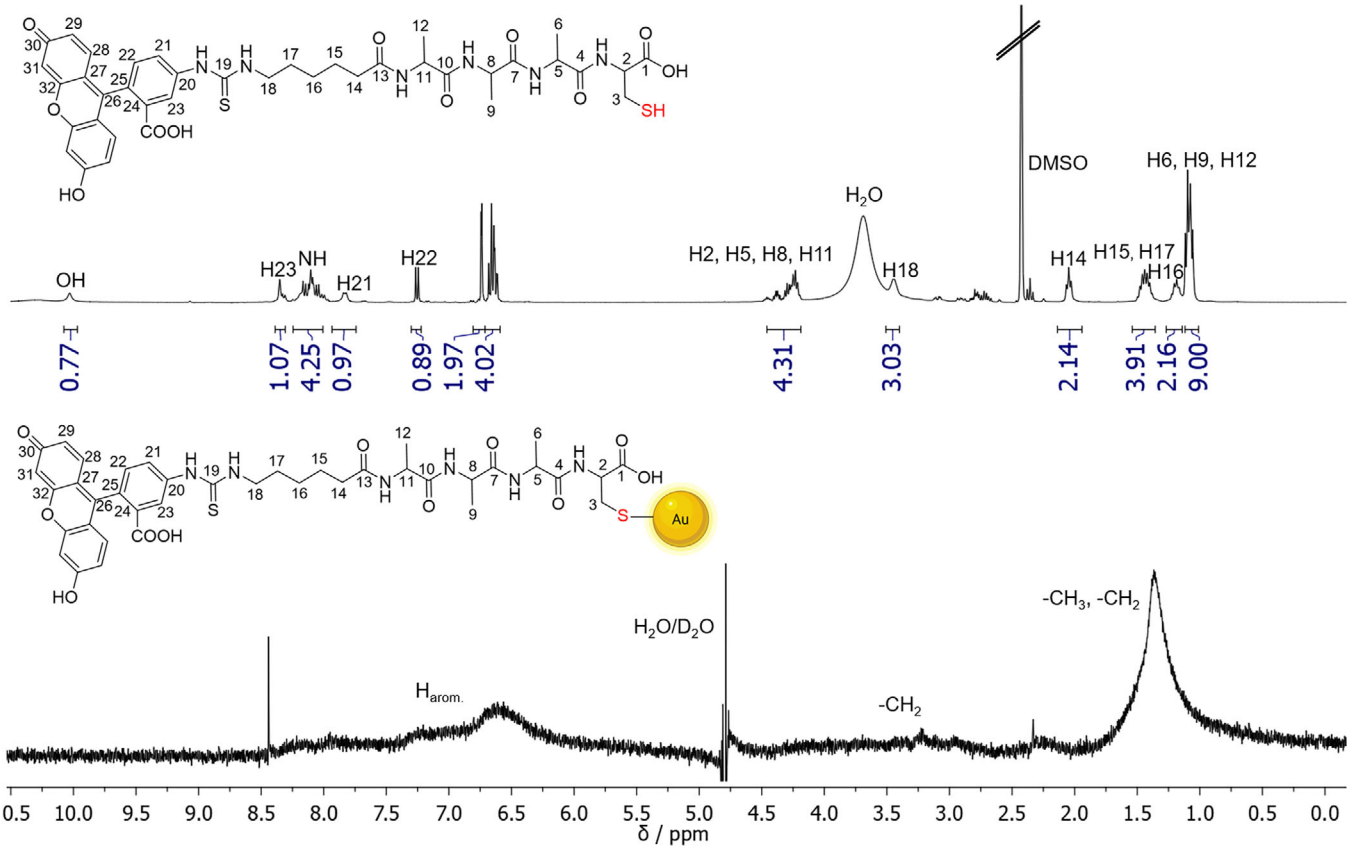

FIGURE 6 | ^{1}H NMR spectra of the ligand CA3-FITC dissolved in DMSO-d_6 (top) and of Au-CA3-FITC nanoparticles dispersed in 10% D_2O/90% H_2O (bottom). The spectra were measured at ambient temperature at 400 MHz.

diameter [46]. This effect becomes stronger for smaller particles and thicker ligand shells, as shown earlier [24, 38]. Unfortunately, neither dynamic light scattering (DLS) nor nanoparticle tracking analysis (NTA) were possible with the ultrasmall nanoparticles. The nanoparticles were too small to scatter the light [47, 48]. Therefore, these experiments could not be carried out.

Infrared spectra of dried nanoparticle samples are shown in Figure 4. They confirm the presence of the ligands.

The successful attachment of the peptides to the nanoparticle surface was confirmed by NMR spectroscopy. NMR spectroscopy is not applicable to larger (plasmonic) nanoparticles because signal intensity and resolution strongly decrease due to the vicinity of the metal core. However, it is a suitable method for ultrasmall nanoparticles, despite the fact that the NMR peaks become broader and are shifted downfield [22, 24, 45, 49, 50]. NMR spectroscopy has also been applied to atom-sharp metal clusters [51]. The free peptides were not sufficiently soluble in H_2O/D_2O due to the aromatic fluorophores, therefore the NMR spectra were recorded in DMSO-d_6. Figure 5 shows the NMR spectra of dispersed Au-CA-FITC nanoparticles and of the dissolved ligand CA-FITC. While the general signal pattern and J-couplings remain, chemical shifts cannot be directly compared between different solvents. In the spectrum of the nanoparticles, a clear peak broadening was observed, suggesting successful binding to the nanoparticle surface. The peak broadening results from a decreased spin-spin relaxation time, which can be attributed to the reduced mobility of the ligands due to their proximity to the metal core [22]. As the spectrum was measured with water suppression at 4.79 ppm, it is possible that neighboring NMR signals were partially suppressed as well.

A distinct peak broadening was also visible for Au-CA3-FITC nanoparticles (Figure 6). Both aliphatic and aromatic signals were broadened, indicating a successful attachment to the surface. As with Au-CA-FITC nanoparticles, it is possible that the water suppression caused the suppression of nearby signals.

Figure 7 shows the NMR spectra of the dissolved peptide WAC and of Au-WAC nanoparticles. The strong peak broadening and the absence of narrow NMR peaks indicated that the conjugation was successful. The NMR spectrum of Au-GSH-AF647 nanoparticles was reported earlier [24].

Au-CA-FITC, Au-CA3-FITC, and Au-GSH-AF647 nanoparticles were colloidally stable in water for several weeks. Only the Au-WAC nanoparticles lost their colloidal stability after 1 day and were, therefore, always freshly prepared and analyzed immediately after synthesis. The chemical stability of the other three types of nanoparticles was investigated during dispersion in water at ambient temperature for up to 7 days by ^{1}H-NMR spectroscopy (see Figures S4–S6). However, the particles were colloidally unstable at high salt concentrations, for example, in PBS, where agglomeration occurred.

^{1}H-DOSY NMR spectroscopy was used to determine the hydrodynamic diameter of water-dispersed nanoparticles [23, 52]. DOSY

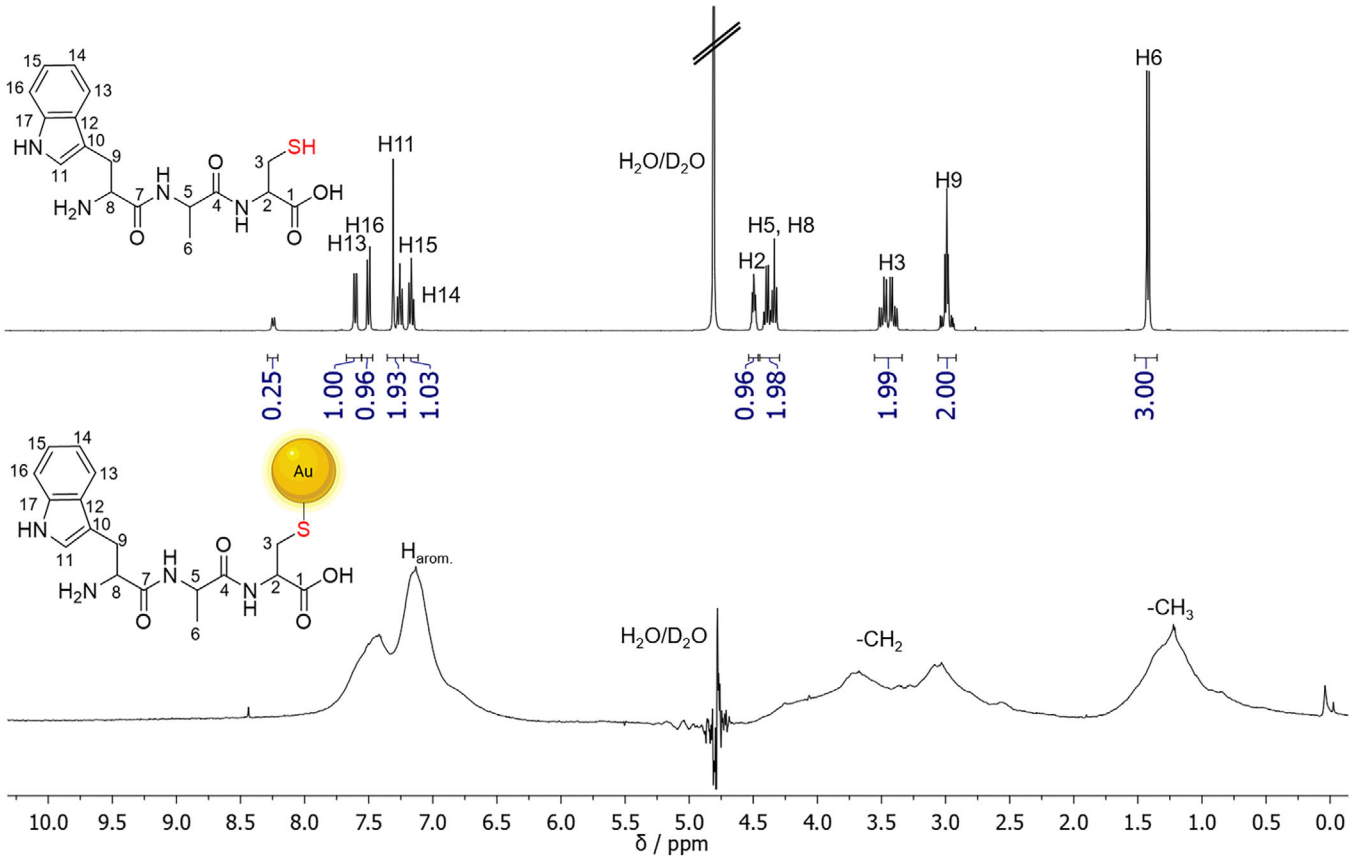

FIGURE 7 | ^{1}H NMR spectra of the ligand WAC dissolved in D_2O (top), and of Au-WAC nanoparticles, dispersed in 10% D_2O/90% H_2O (bottom). The spectra were measured at ambient temperature at 400 MHz.

can distinguish between free ligands and surface-bound ligands as they have different diffusion coefficients. Figure 8 shows the Stejskal–Tanner plots of the ^{1}H-DOSY NMR spectra of all nanoparticles [53]. The hydrodynamic diameters were calculated with the Stokes-Einstein equation from the diffusion coefficients, giving hydrodynamic diameters of 2.2 ± 0.4 nm and 3.5 ± 0.7 nm for Au-CA-FITC and Au-CA3-FITC, respectively. For comparison, hydrodynamic diameters of 3.1 and 3.8 nm were determined earlier for Au-CA and Au-CA3 nanoparticles, respectively [45]. Au-WAC nanoparticles had a hydrodynamic diameter of 3.0 ± 0.6 nm. These values are higher than those obtained by DCS because DOSY determines the "true" hydrodynamic diameter. Of course, they are also higher than the diameters of the gold core alone, as assessed by TEM. No NMR peaks of dissolved ligands were observed by DOSY.

UV-Vis spectroscopy gave the absorption characteristics of all nanoparticles. Plasmonic gold particles have a surface plasmon resonance (SPR) band at approximately 520 nm [6, 54, 55]. However, no plasmon band was present in any spectrum (Figure 9), confirming the absence of plasmonic gold nanoparticles. Au-CA-FITC nanoparticles and Au-CA3-FITC nanoparticles showed the band of FITC at 493 nm. Au-WAC nanoparticles showed the band of tryptophan at 280 nm. Au-GSH-AF647 nanoparticles showed the band of AF647 at 647 nm. These absorption bands were used to determine the number of attached ligands on each nanoparticle.

To determine the number of ligands per nanoparticle, AAS, ICP-MS, UV-Vis spectroscopy, and NMR spectroscopy were used [24, 56]. The quantification for Au-WAC nanoparticles was performed by NMR spectroscopy and UV-Vis spectroscopy, while UV-Vis spectroscopy was chosen for the nanoparticles labeled with FITC.

Quantification by NMR spectroscopy was performed by adding maleic acid as an internal standard to a dispersion of Au-WAC nanoparticles [24, 45]. The ligand concentration was determined by integration and considering the integrality of the methyl protons (H6) from 0.6 to 1.9 ppm (Figure S1). The nanoparticle concentration was obtained from the gold concentration determined by AAS in all cases. Spherical particles with a diameter of 2 nm and approximately 250 atoms were assumed based on the HRTEM results (see Ref. [24] for details of this computation). The number of ligands was then calculated from the molar ratio of ligands and nanoparticles in a given dispersion. By quantitative ^{1}H-NMR spectroscopy, 65 WAC molecules were attached to each particle. UV-Vis spectroscopy gave 53 WAC molecules per nanoparticle (Figure S2). The molecular footprint of WAC was computed with the nanoparticle surface, giving 0.19 nm^2 (from NMR data) and 0.24 nm^2 (from UV-Vis data) for WAC. These results are in good agreement with previously determined values by ^{1}H NMR spectroscopy for other tripeptides ACA (0.29 nm^2) and CAA (0.25 nm^2) [45].

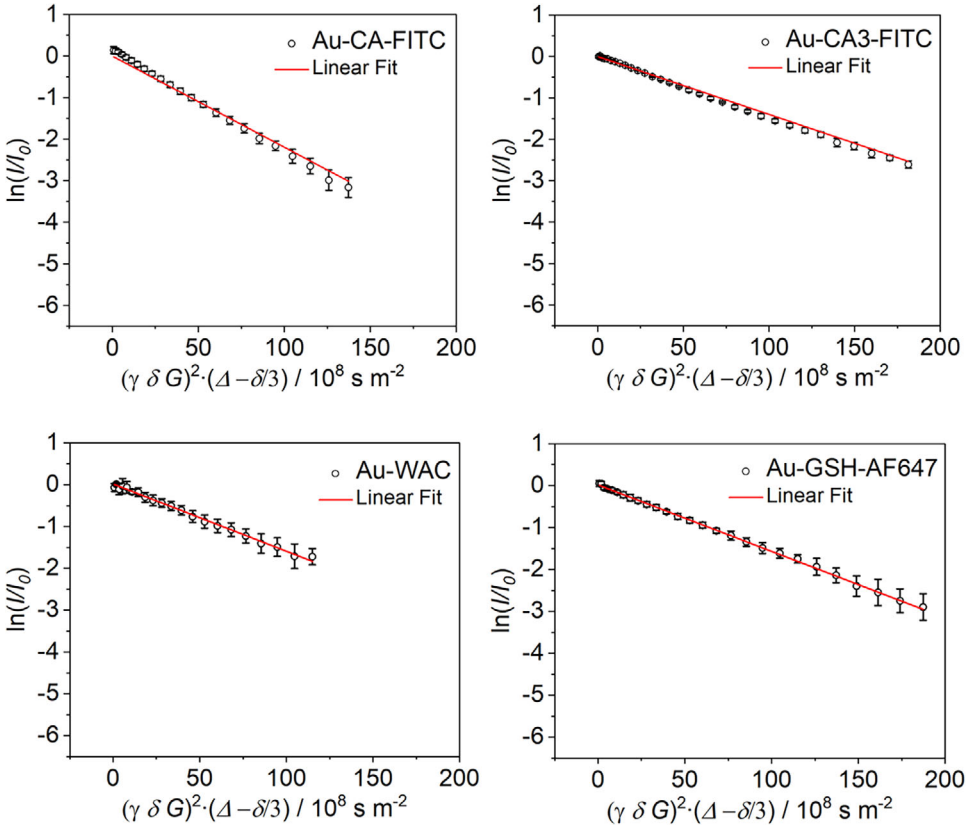

FIGURE 8 | Stejskal–Tanner plots of ^{1}H-DOSY NMR experiments of labeled gold nanoparticles dispersed in 10% D_2O/90% H_2O. The negative slope corresponds to the diffusion coefficient.

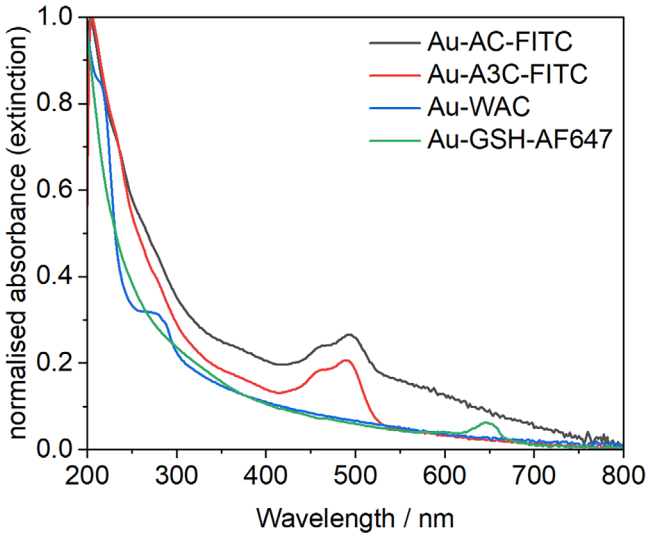

FIGURE 9 | UV-Vis spectra of peptide-conjugated ultrasmall gold nanoparticles, dispersed in water. No plasmon resonance band at 520 nm was detected, confirming the absence of larger (plasmonic) gold nanoparticles.

Quantification of the ligand number on Au-CA-FITC and Au-CA3-FITC nanoparticles was performed by UV-Vis spectroscopy only as the NMR signals were difficult to integrate (Figure S3) [24]. This resulted in 19 ligands per particle for Au-CA-FITC with a molecular footprint of 0.67 nm^2 and 15 ligands per particle for Au-CA3-FITC with a molecular footprint of 0.84 nm^2. Notably, the footprint of the corresponding unlabeled peptides CA and CA3 was much smaller, that is, 0.12 and 0.32 nm^2, respectively [45], than that of the FITC-labeled peptides studied here. Not unsurprisingly, given the size of FITC in comparison to the peptide, FITC has a major steric influence (see also Figure 1), and consequently, fewer peptide ligands are bound to the surface. In good agreement with the tripeptide GSH carrying a fluorescent dye, Au-GSH-AF647 nanoparticles carried 11 AF647 molecules on each 2 nm gold nanoparticle with a molecular footprint of 1.15 nm^2, as reported earlier [24]. All characterization data are summarized in Table 1.

We emphasize that all spectroscopic experiments were carried out at the same concentration of the fluorophore. As each kind of nanoparticle carries different numbers of dye molecules, it is not possible to perform all experiments at the same dye concentration and the same nanoparticle concentration. The data in Table 1 permit the conversion of dye concentrations to nanoparticle concentrations, if necessary. The fluorescence intensities were measured from 25°C to 85°C (Figure 10). The aim was to investigate the impact of increased thermal dynamics of the attached ligands on the emission intensities of the fluorophore. The same molar concentration of FITC was used for CA-FITC, CA3-FITC, Au-CA-FITC, and Au-CA3-FITC. For the FITC-labeled peptides, the fluorescence intensities at 25°C were identical, as expected. After attachment to the nanoparticles, the fluorescence intensities fell to about one-half for FITC-labeled

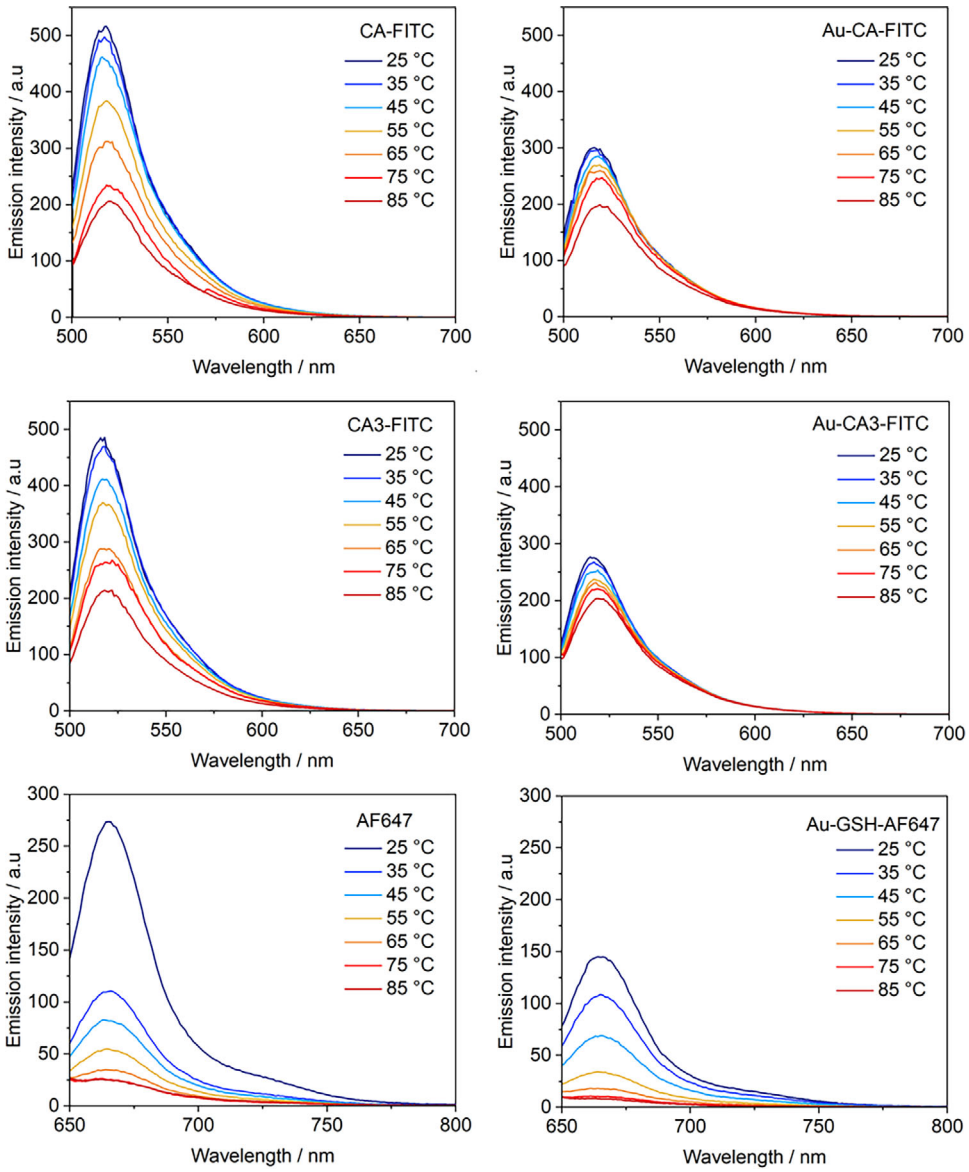

FIGURE 10 | Fluorescence emission spectra of CA-FITC, Au-CA-FITC nanoparticles, CA3-FITC, Au-CA3-FITC nanoparticles, AF647, and Au-GSH-AF647 nanoparticles at different temperature in water (pH = 7). The concentration of FITC was 3 μM in all cases. The concentration of AF647 was 1 μM.

peptides. Obviously, the difference in the distance between the fluorophore and the metal surface was too small to induce a significant difference between the two peptides. Similarly, the fluorescence intensity of AF647 decreased by a factor of about 2 after conjugation to the gold nanoparticle.

A considerable decrease in fluorescence with increasing temperature was observed for all attached and free ligands. This temperature-dependent effect can be attributed to various factors, including increased molecular collisions and enhanced internal conversion processes [57–60]. The integrated fluorescence intensity of all ligands and nanoparticles as a function of temperature is shown in Figure 11. Remarkably, the decrease in fluorescence with increasing temperature was significantly smaller for particle-bound FITC than for the free ligands. With increasing temperature, the intensities became similar, that is, the fluorescence of free and conjugated peptide-FITC was almost equal at 85°C. This effect may be due to a restricted mobility of dyes on the nanoparticle surface, leading to higher quenching than with free dyes. In other words, the loss of fluorescence at higher temperature has already occurred on the nanoparticle-bound dyes at ambient temperature and is, therefore, less temperature-dependent than on dissolved molecular dyes. In contrast, the fluorescence intensity of free and conjugated AF647 decreased significantly with increasing temperature in the same way. However, the fluorescence intensity was always higher for the free ligands than for the nanoparticle-conjugated ligands. Obviously, the quenching depends on the fluorophore.

The fluorescence intensity was fully recovered after cooling back to ambient temperature. This indicates that no permanent change had occurred during the heating process, that is, the particle-peptide conjugation was stable. This was also the case for the

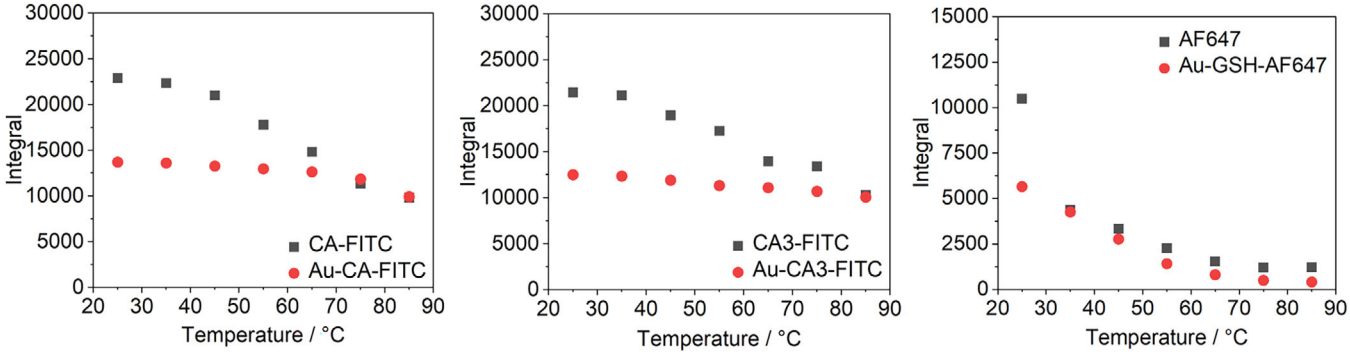

FIGURE 11 | Comparison of the integrated emission bands from fluorescence spectroscopy (data taken from Figure 10). A decrease with increasing temperature was observed for both dissolved dyes and conjugated dyes on the surface of nanoparticles.

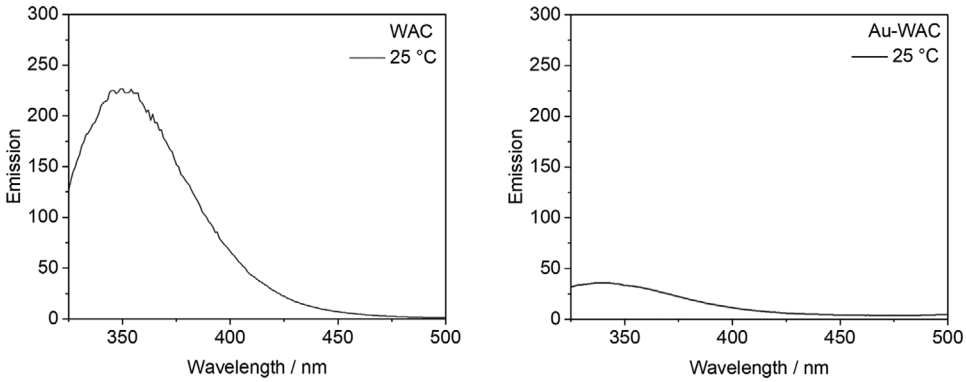

FIGURE 12 | Fluorescence emission spectra of free WAC (left) and Au-WAC nanoparticles (right) at a concentration of 0.5 mM in water (pH 7).

labeled peptides, which were stable during heating (see Figures S7–S10).

The tripeptide WAC showed a weaker fluorescence. Here, an almost complete loss of intrinsic fluorescence was observed after binding to the metal core (Figure 12). This is remarkable, given the much higher number of attached fluorophores for Au-WAC nanoparticles in comparison to the other nanoparticles (about 60 vs. about 10–20). An explanation could be the low distance between the metal core and fluorophore, which is the lowest of all investigated nanoparticles (see Figure 1). Another explanation could be π-π-stacking between indole rings in adjacent tryptophanes. Finally, it is possible that the absorption of the nanoparticles in the near UV range (see Figure 9) decreases the fluorescence from tryptophan at 360 nm.

The absolute photoluminescence quantum yield (Φ_{PL}) allows a more quantitative understanding of the influence of the metal core on the emissive behavior (Figure 13 and Table 2). The determined value of 89% for the free ligand AC-FITC is in good agreement with the literature value of 92% for FITC, within the margin of error [31, 34]. For the free ligand CA3-FITC, the Φ_{PL} value was 65%, possibly due to the longer peptide chain and an associated quenching effect. The quantum yield dropped to 7% for Au-CA-FITC and 3% for Au-CA3-FITC nanoparticles after attachment to the metal cores. The Φ_{PL} value of 23% for AF647 was below the value of 33% reported in the literature [31] but dropped only slightly to 20% for Au-GSH-AF647. Free WAC showed an expectedly low Φ_{PL} value of 6%, in good agreement with the literature [61]. However, it was essentially zero after conjugation to the gold nanoparticles.

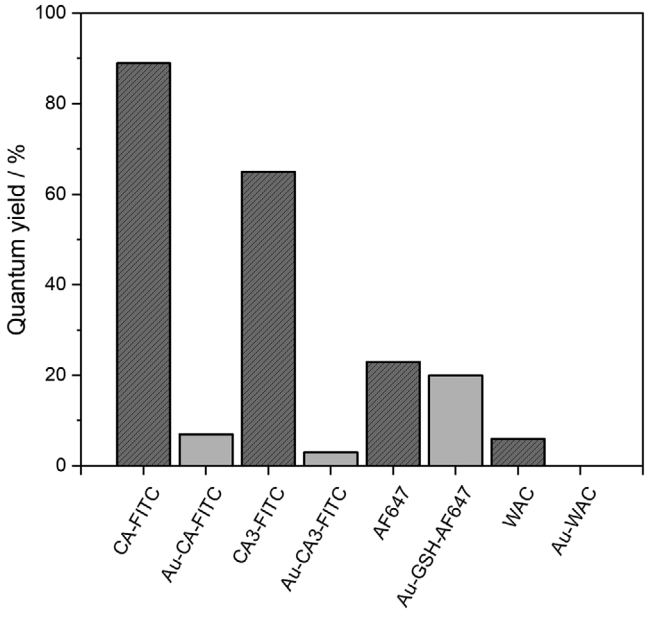

FIGURE 13 | Absolute photoluminescence quantum yields (Φ_{PL}) of free and nanoparticle-conjugated ligands, determined for solutions and dispersions (3 μM) in water (pH 7). A clear decrease was evident due to the attachment of the dyes to the nanoparticle surface.

TABLE 1 | Summary of the characterization data of all investigated fluorescently labeled ultrasmall gold nanoparticles.

Nanoparticle	Hydrodynamic diameter by DCS/nm	Hydrodynamic diameter by ^{1}H-DOSY NMR/nm	Core diameter by HRTEM/nm	Number of ligands per particle (based on 2 nm diameter)	Molecular footprint of each ligand/nm^2	Absorption maximum by UV-Vis/nm	Reference
Au-CA-FITC	1.3 ± 0.3	2.2 ± 0.4	1.6 ± 0.6	19	0.67	493	This work
Au-CA	1.5 ± 0.4	3.1 ± 0.6	2.1 ± 0.8	105	0.12	—	[45]
Au-CA3-FITC	1.3 ± 0.3	3.5 ± 0.7	1.1 ± 0.4	15	0.84	493	This work
Au-CA3	1.3 ± 0.2	3.8 ± 0.8	2.2 ± 0.6	39	0.32	—	[45]
Au-WAC	1.3 ± 0.2	3.0 ± 0.6	1.7 ± 0.4	65 (NMR) 53 (UV-Vis)	0.19 (NMR) 0.24 (UV-Vis)	280	This work
Au-GSH-AF647	1.4 ± 0.3	3.1 ± 0.6	2.5 ± 1.1	11	1.15	647	This work (DCS, DOSY); [24]

TABLE 2 | Summary of all determined absolute photoluminescence quantum yield values (Φ_{PL}) of all molecules and particles (measured in water, 3 μM fluorophore concentration, pH 7). The estimated error in Φ_{PL} is 2%.

	Φ_{PL}/%	Reference
FITC	93	[31]
CA-FITC	89	This work
Au-CA-FITC	7	This work
CA3-FITC	65	This work
Au-CA3-FITC	3	This work
AF647	33	[31]
AF647	23	This work
Au-GSH-AF647	20	This work
W (tryptophan)	13	[61]
WAC	6	This work
Au-WAC	0	This work

Note that the estimation of the photoluminescence quantum yield from the decrease in emission spectra must be handled with caution. The absolute photoluminescence quantum yield was measured with an integrated Ulbricht sphere (i.e., not with the relative method). It is defined as the ratio of emitted photons to absorbed photons. Since the absorption properties of a dye change upon attachment to a nanoparticle, the Φ_{PL} value will change as well. Also, it is not the emission maximum, but the area that is used to determine the quantum yield, therefore, a decrease of 50% is not corresponding to a quenching of 50%. Keeping that in mind, a direct correlation between emission intensity and peak width with the absolute photoluminescence quantum yields is not possible.

Fluorescence and quenching depend on the fluorophore and the intrinsic quantum yield [62]. In general, the conjugation of the ligands to the gold nanoparticles led to a significant loss of intensity, but not to a complete quenching as with plasmonic particles. Yun et al. investigated the energy transfer processes in non-plasmonic nanoparticles, denoted as nanosurface energy transfer (NSET). This involves the transfer of energy from a molecular dipole to the surface of a nanometer-sized metal. In particular, the enhanced quenching is related to the fact that the energy transfer from a dye to a metallic nanoparticle is most efficient when there is an overlap between the emission band of the donor and the absorption band of the nanoparticle. This overlap corresponds to the regions where NSET causes the strongest quenching effect [63]. Dulkeith et al. investigated dye-functionalized nanoparticles of different sizes. They described the quenching mechanism as an NSET for small particles of <2 nm [30]. Jennings et al. investigated DNA-functionalized nanoparticles with a diameter of 1.5 nm, where DNA determined the distance between the fluorophore and the particle surface. Again, the efficiency of quenching depended strongly on the overlap between the emission wavelength of the dye and the absorption transitions of the gold nanoparticle. In the absence of plasmon resonance, quenching is based on the interaction of the dye and the electronic states of the metal. The study

confirmed that non-plasmonic gold nanoparticles can act as energy-absorbing structures like a macroscopic metal surface [29].

Wang et al. calculated the theoretical quantum yields of different dyes bound to 30 nm gold nanoparticles. They found that the quantum yields were lowest near the metal core and increased with distance. For certain dyes, such as FITC or Cy3, the values were very low even at a distance of 10 nm, while for AF647 or AF700, the quantum yields were similar to the free ligand. This effect is due to the similar emission wavelength of FITC (521 nm) and Cy3 (555 nm) to the absorption band the plasmonic nanoparticles, while AF647 (665 nm) and AF700 (723 nm) emit at significantly higher wavelengths [31, 62]. Thus, the quenching efficiency depends not only on the distance between the dye and the particle but also on the emission wavelength of the dye. It is highest when the emission of the dye overlaps with the specific absorption transitions of the gold nanoclusters or nanoparticles [28, 30].

Although the particles that were studied here are not plasmonic, the quenching effect was strong in all cases, illustrating the energy transfer from the excited fluorophore to the metallic nanoparticles, leading to non-radiative energy transfer. Notably, this effect becomes weaker at elevated temperature, where dissolved dyes lose their fluorescence more rapidly than conjugated dyes.

4 | Conclusions

The fluorescence intensity of dyes that are covalently attached to ultrasmall gold nanoparticles decreases considerably due to the presence of the metal core. This is the case for two FITC-labeled peptides and the dye AlexaFluor-647. The intrinsically fluorescent peptide WAC, where tryptophan is the fluorophore, is completely quenched after attachment to the gold nanoparticle. This shows that even ultrasmall (non-plasmonic) nanoparticles can lead to a considerable quenching, although the extent is much smaller than in plasmonic nanoparticles, for example, 10–20 nm in diameter. Plasmonic nanoparticles can only be labeled with very long spacers between the metal surface and fluorophore, leading to rather a thick shell around the nanoparticle core. In the cases investigated here, the distance between the metal surface and fluorophore was in the range of 1 to 2 nm. Therefore, ultrasmall nanoparticles are useful as fluorescent probes, for example, to trace them inside cells or tissues, but their fluorescence is significantly lower than that of the free dyes. An advantage, for example, for the mobility in biological systems, is that their small size increases from about 2 nm (metallic core) to 4 nm (hydrodynamic diameter) after attachment of the fluorescent layer. Fluorescently labeled short peptides are convenient ligands to stabilize ultrasmall nanoparticles via the Au-S bond formed by cysteine.

Acknowledgments

We thank Mr. Robin Meya for AAS analyses. We thank Dr. Torsten Schaller and Dr. Felix Niemeyer for support with NMR spectroscopy.

Conflicts of Interest

The authors declare no conflicts of interest.

Data Availability Statement

All data generated or analyzed during this study are included in this published article and its Supporting Information files.

References

1. G. Yang, Z. P. Wang, F. L. Du, F. Y. Jiang, X. Yuan, and J. Y. Ying, "Ultrasmall Coinage Metal Nanoclusters as Promising Theranostic Probes for Biomedical Applications," *Journal of the American Chemical Society* 145 (2023): 11879–11898.

2. S. Roy, I. Hasan, and B. Guo, "Recent Advances in Nanoparticle-Mediated Antibacterial Applications," *Coordination Chemistry Reviews* 482 (2023): 215075.

3. C. B. Gao, F. L. Lyu, and Y. D. Yin, "Encapsulated Metal Nanoparticles for Catalysis," *Chemical Reviews Journal* 121 (2021): 834–881.

4. C. J. Zeng, "Precision at the Nanoscale: On the Structure and Property Evolution of Gold Nanoclusters," *Pure and Applied Chemistry* 90 (2018): 1409–1427.

5. L. C. Liu and A. Corma, "Metal Catalysts for Heterogeneous Catalysis: From Single Atoms to Nanoclusters and Nanoparticles," *Chemical Reviews Journal* 118 (2018): 4981–5079.

6. R. Yu, L. M. Liz-Marzan, and F. J. Garcia de Abajo, "Universal Analytical Modeling of Plasmonic Nanoparticles," *Chemical Society Reviews* 46 (2017): 6710–6724.

7. J. C. Hsu, D. Barragan, A. E. Tward, et al., "A Biodegradable "One-For-All" Nanoparticle for Multimodality Imaging and Enhanced Photothermal Treatment of Breast Cancer," *Advanced Healthcare Materials* 13 (2024): 2303018.

8. T. J. Liu, L. L. Tong, N. N. Lv, et al., "Two-Stage Size Decrease and Enhanced Photoacoustic Performance of Stimuli-Responsive Polymer-Gold Nanorod Assembly for Increased Tumor Penetration," *Advanced Functional Materials* 29 (2019): 1806429.

9. X. G. Ge, B. Chen, T. J. Liu, et al., "Active Targeting Drug-Gold Nanorod Hybrid Nanoparticles for Amplifying Photoacoustic Signal and Enhancing Anticancer Efficacy," *RSC Advances* 9 (2019): 13494–13502.

10. L. Josephson, M. F. Kircher, U. Mahmood, Y. Tang, and R. Weissleder, "Near-Infrared Fluorescent Nanoparticles as Combined MR/Optical Imaging Probes," *Bioconjugate Chemistry* 13 (2002): 554–560.

11. K. Zarschler, L. Rocks, N. Licciardello, et al., "Ultrasmall Inorganic Nanoparticles: State-of-the-Art and Perspectives for Biomedical Applications," *Nanomedicine* 12 (2016): 1663–1701.

12. M. Epple, V. M. Rotello, and K. Dawson, "The Why and How of Ultrasmall Nanoparticles," *Accounts of Chemical Research* 56 (2023): 3369–3378.

13. M. Zhou, X. Du, H. Wang, and R. Jin, "The Critical Number of Gold Atoms for a Metallic State Nanocluster: Resolving a Decades-Long Question," *ACS Nano* 15 (2021): 13980–13992.

14. A. A. Sousa, P. Schuck, and S. A. Hassan, "Biomolecular Interactions of Ultrasmall Metallic Nanoparticles and Nanoclusters," *Nanoscale Advances* 3 (2021): 2995–3027.

15. F. Muraca, L. Boselli, V. Castagnola, and K. A. Dawson, "Ultrasmall Gold Nanoparticle Cellular Uptake: Influence of Transient Bionano Interactions," *ACS Applied Bio Materials* 3 (2020): 3800–3808.

16. L. S. Wagner, T. Thiele, K. Loza, et al., "Ultrasmall Gold Nanoparticles (2 nm) Decorated with a High Density of Photochemically Switchable Ligands," *Chemistry – A European Journal* (2025): e202501204.

17. K. Kostka, V. Sokolova, A. El-Taibany, et al., "The Application of Ultrasmall Gold Nanoparticles (2 nm) Functionalized with Doxorubicin

in Three-Dimensional Normal and Glioblastoma Organoid Models of the Blood–Brain Barrier," *Molecules (Basel, Switzerland)* 29 (2024): 2469.

18. V. Sokolova, J. F. Ebel, S. Kollenda, et al., "Uptake of Functional Ultrasmall Gold Nanoparticles in 3D Gut Cell Models," *Small* 18 (2022): 2201167.

19. M. Fan, Y. Han, S. T. Gao, et al., "Ultrasmall Gold Nanoparticles in Cancer Diagnosis and Therapy," *Theranostics* 10 (2020): 4944–4957.

20. X. Zhang, S. Shastry, S. E. Bradforth, and J. L. Nadeau, "Nuclear Uptake of Ultrasmall Gold-Doxorubicin Conjugates Imaged by Fluorescence Lifetime Imaging Microscopy (FLIM) and Electron Microscopy," *Nanoscale* 7 (2015): 240–251.

21. N. Wolff, C. Beuck, T. Schaller, and M. Epple, "Possibilities and Limitations of Solution-State NMR Spectroscopy to Analyze the Ligand Shell of Ultrasmall Metal Nanoparticles," *Nanoscale Advances* 6 (2024): 3285–3298.

22. L. E. Marbella and J. E. Millstone, "NMR Techniques for Noble Metal Nanoparticles," *Chemistry of Materials* 27 (2015): 2721–2739.

23. G. Salassa and T. Burgi, "NMR Spectroscopy: A Potent Tool for Studying Monolayer-Protected Metal Nanoclusters," *Nanoscale Horizons* 3 (2018): 457–463.

24. K. Klein, K. Loza, M. Heggen, and M. Epple, "An Efficient Method for Covalent Surface Functionalization of Ultrasmall Metallic Nanoparticles by Surface Azidation, Followed by Copper-Catalyzed Azide-Alkyne Cycloaddition," *ChemNanoMat* 7 (2021): 1330–1339.

25. B. Kruse, B. S. Dash, K. Kostka, et al., "Doxorubicin-Loaded Ultrasmall Gold Nanoparticles (1.5 nm) for Brain Tumor Therapy and Assessment of Their Biodistribution," *ACS Applied Bio Materials* 7 (2024): 6890–6907.

26. C. Xue, Y. Xue, L. Dai, A. Urbas, and Q. Li, "Size- and Shape-Dependent Fluorescence Quenching of Gold Nanoparticles on Perylene Dye," *Advanced Optical Materials* 1 (2013): 581–587.

27. M. J. Cui, H. M. Lu, H. P. Jiang, Z. H. Cao, and X. K. Meng, "Phase Diagram of Continuous Binary Nanoalloys: Size, Shape, and Segregation Effects," *Scientific Reports* 7 (2017): 41990.

28. S. Chowdhury, Z. Wu, A. Jaquins-Gerstl, et al., "Wavelength Dependence of the Fluorescence Quenching Efficiency of Nearby Dyes by Gold Nanoclusters and Nanoparticles: The Roles of Spectral Overlap and Particle Size," *Journal of Physical Chemistry C* 115 (2011): 20105–20112.

29. T. L. Jennings, M. P. Singh, and G. F. Strouse, "Fluorescent Lifetime Quenching Near D = 1.5 Nm Gold Nanoparticles: Probing NSET Validity," *Journal of the American Chemical Society* 128 (2006): 5462–5467.

30. E. Dulkeith, A. C. Morteani, T. Niedereichholz, et al., "Fluorescence Quenching of Dye Molecules near Gold Nanoparticles: Radiative and Nonradiative Effects," *Physical Review Letter* 89 (2002): 203002.

31. J. Wang, S. Achilefu, M. Nantz, and K. A. Kang, "Gold Nanoparticle-Fluorophore Complex for Conditionally Fluorescing Signal Mediator," *Analytica Chimica Acta* 695 (2011): 96–104.

32. R. Chhabra, J. Sharma, H. Wang, et al., "Distance-Dependent Interactions Between Gold Nanoparticles and Fluorescent Molecules with DNA as Tunable Spacers," *Nanotechnology* 20 (2009): 485201.

33. K. A. Kang, J. Wang, J. B. Jasinski, and S. Achilefu, "Fluorescence Manipulation by Gold Nanoparticles: From Complete Quenching to Extensive Enhancement," *Journal of Nanbiotechnology* 9 (2011): 16.

34. J. Wang, J. Moore, S. Laulhe, M. Nantz, S. Achilefu, and K. A. Kang, "Fluorophore-Gold Nanoparticle Complex for Sensitive Optical Biosensing and Imaging," *Nanotechnology* 23 (2012): 095501.

35. B. N. J. Persson and N. D. Lang, "Electron-Hole-Pair Quenching of Excited States Near a Metal," *Physical Review B* 26 (1982): 5409–5415.

36. T. Ruks, K. Loza, M. Heggen, et al., "Peptide-Conjugated Ultrasmall Gold Nanoparticles (2 nm) for Selective Protein Targeting," *ACS Applied Bio Materials* 4 (2021): 945–965.

37. T. Ruks, K. Loza, M. Heggen, et al., "Targeting the Surface of the Protein 14-3-3 by Ultrasmall Gold Nanoparticles (1.5 nm), Carrying the Specific Peptide CRaf," *Chembiochem* 22 (2021): 1456–1463.

38. N. Wolff, S. Kollenda, K. Klein, et al., "Silencing of Proinflammatory NF-κB and Inhibition of Herpes Simplex Virus (HSV) Replication by Ultrasmall Gold Nanoparticles (2 nm) Conjugated with Small-Interfering RNA," *Nanoscale Advances* 4 (2022): 4502–4516.

39. P. Stahl, S. Kollenda, J. Sager, et al., "Tuning Nanobodies' bioactivity: Coupling to Ultrasmall Gold Nanoparticles Allows the Intracellular Interference with Survivin," *Small* 13 (2023): 2300871.

40. S. B. van der Meer, T. Seiler, C. Buchmann, et al., "Controlling the Surface Functionalization of Ultrasmall Gold Nanoparticles by Sequence-Defined Macromolecules," *Chemistry – A European Journal* 27 (2021): 1451–1464.

41. N. Wolff, N. Bialas, K. Loza, et al., "Increased Cytotoxicity of Bimetallic Ultrasmall Silver–Platinum Nanoparticles (2 nm) on Cells and Bacteria in Comparison to Silver Nanoparticles of the Same Size," *Materials* 17 (2024): 3702.

42. J. Barthel, L. Houben, and K. Tillmann, "FEI Titan G3 50–300 PICO," *Journal of Large-Scale Research Facilities* 1 (2015): A34.

43. N. Gumbiowski, K. Loza, M. Heggen, and M. Epple, "Automated Analysis of Transmission Electron Micrographs of Metallic Nanoparticles by Machine Learning," *Nanoscale Advances* 5 (2023): 2318–2326.

44. M. Brust, J. Fink, D. Bethell, D. J. Schiffrin, and C. Kiely, "Synthesis and Reactions of Functionalised Gold Nanoparticles," *Chemical Communications* (1995): 1655.

45. L. S. Wagner, O. Prymak, T. Schaller, et al., "The Molecular Footprint of Peptides on the Surface of Ultrasmall Gold Nanoparticles (2 nm) Is Governed by Steric Demand," *Journal of Physical Chemistry B* 128 (2024): 4266–4281.

46. H. Fissan, S. Ristig, H. Kaminski, C. Asbach, and M. Epple, "Comparison of Different Characterization Methods for Nanoparticle Dispersions Before and After Aerosolization," *Analytical Methods* 6 (2014): 7324.

47. R. T. Coones, V. Kestens, and C. Minelli, "A Comparison of Hydrodynamic Diameter Results from MADLS and DLS Measurements for Nanoparticle Reference Materials," *Journal of Nanoparticle Research* 27 (2025): 170.

48. M. M. Modena, B. Rühle, T. P. Burg, and S. Wuttke, "Nanoparticle Characterization: What to Measure?," *Advanced Materials* 31 (2019): 1901556.

49. B. Schuetze, C. Mayer, K. Loza, M. Gocyla, M. Heggen, and M. Epple, "Conjugation of Thiol-Terminated Molecules to Ultrasmall 2 Nm-Gold Nanoparticles Leads to Remarkably Complex ^{1}H-NMR Spectra," *Journal of Materials Chemistry B* 4 (2016): 2179–2189.

50. T. Ruks, C. Beuck, T. Schaller, et al., "Solution NMR Spectroscopy with Isotope-labelled Cysteine (^{13}C, ^{15}N) Reveals the Surface Structure of L-Cysteine-Coated Ultrasmall Gold Nanoparticles (1.8 nm)," *Langmuir* 35 (2019): 767–778.

51. K. Salorinne, S. Malola, O. A. Wong, et al., "Conformation and Dynamics of the Ligand Shell of a Water-Soluble Au_{102} Nanoparticle," *Nature Communications* 7 (2016): 10401.

52. K. Salorinne, T. Lahtinen, J. Koivisto, et al., "Nondestructive Size Determination of Thiol-Stabilized Gold Nanoclusters in Solution by Diffusion Ordered NMR Spectroscopy," *Analytical Chemistry* 85 (2013): 3489–3492.

53. E. O. Stejskal and J. E. Tanner, "Spin Diffusion Measurements: Spin Echoes in the Presence of a Time-Dependent Field Gradient," *Journal of Chemical Physics* 42 (1965): 288–292.

54. V. Amendola, R. Pilot, M. Frasconi, O. M. Marago, and M. A. Iati, "Surface Plasmon Resonance in Gold Nanoparticles: A Review," *Journal of Physics: Condensed Matter* 29 (2017): 203002.

55. J. Langer, S. M. Novikov, and L. M. Liz-Marzan, "Sensing Using Plasmonic Nanostructures and Nanoparticles," *Nanotechnology* 26 (2015): 322001.

56. N. Wolff, K. Loza, M. Heggen, et al., "Ultrastructure and Surface Composition of Glutathione-Terminated Ultrasmall Silver, Gold, Platinum, and Alloyed Silver–Platinum Nanoparticles (2 nm)," *Inorganic Chemistry* 62 (2023): 17470–17485.

57. H. R. Deepa, J. Thipperudrappa, and H. M. Suresh Kumar, "Effect of Temperature on Fluorescence Quenching and Emission Characteristics of Laser Dyes," *Journal of Physics: Conference Series* 1473 (2020): 012046.

58. T. Liu, J. Huang, H. Ding, C. Zhan, and S. Wang, "Molecular Structure Perspective on Temperature-Sensitive Properties of Rhodamine Aqueous Solutions," *Spectrochim Acta A* 275 (2022): 121166.

59. M. M. Martin, "Intermolecular Hydrogen Bonding and Temperature Effects on Internal Conversion in Xanthene Dyes," *Chemical Physics Letters* 43 (1976): 332–337.

60. A. Lindstaedt, J. Doroszuk, A. Machnikowska, et al., "Effects Induced by the Temperature and Chemical Environment on the Fluorescence of Water-Soluble Gold Nanoparticles Functionalized with a Perylene-Derivative Dye," *Materials* (2024): 17.

61. R. F. Chen, "Fluorescence Quantum Yields of Tryptophan and Tyrosine," *Analytical Letters* 1 (1967): 35–42.

62. M. Cui, Y. Zhao, and Q. Song, "Synthesis, Optical Properties and Applications of Ultra-Small Luminescent Gold Nanoclusters," *Trends in Analytical Chemistry* 57 (2014): 73–82.

63. C. S. Yun, A. Javier, T. Jennings, et al., "Nanometal Surface Energy Transfer in Optical Rulers, Breaking the FRET Barrier," *Journal of the American Chemical Society* 127 (2005): 3115–3119.

Supporting Information

Additional supporting information can be found online in the Supporting Information section.

Supporting File 1: nano70041-sup-0001-SuppMat.pdf.